communications earth & environment

Article

A Nature Portfolio journal

https://doi.org/10.1038/s43247-026-03307-3

Deciphering the origin of electron exchange capacities in floodplain sediments

Chenglong Yu[1], Shengyan Pu[1,2] ✉, Bo Li[1], Lijun Fan[1], Peng Zhang[3], Fengchang Wu[2] ✉ & Andreas Kappler[4]

Floodplain sediments play a central role in redox-driven biogeochemical cycles through their electron exchange capacity, yet its origin remains unclear because of strong chemical heterogeneity. Here we quantified the electron-accepting and electron-donating capacities of 45 sediments from two Yangtze River floodplains using mediated electrochemical analysis. We identified that electron-accepting capacity was controlled by acid-extractable reactive ferric iron associated with iron (oxyhydr)oxides and expandable phyllosilicates. Electron-donating capacity was mainly contributed by terrigenous humic fractions (12.9–61.2%) and reactive ferrous iron (38.8–87.1%). Lignin-like compounds with low double bond equivalent were the dominant organic contributors to electron-donating capacity. For ferrous iron, its contribution to sediment electron-donating capacity was much smaller than predicted by chemometric analysis because a large fraction of ferrous iron associated with phyllosilicates was redox-inert due to chemical and structural constraints. The composition of electron exchange capacity dictated microbial selection of terminal electron acceptors, driving the conversion of high-redox-potential electron-accepting capacity into electron-donating capacity. This transformation of electron exchange capacity has important implications for suppressing methanogenesis in floodplains and for oxidant consumption during contaminated aquifer remediation.

Floodplains, covering approximately 15 million km^2 globally[1], are among the most widespread terrestrial ecosystems on Earth. The sediment–groundwater systems in floodplains are hotspots for biogeochemical processes, including elemental cycling, nutrient and contaminant transformations, and greenhouse gas emissions, which profoundly impact water quality, agriculture, and climate change[2]. Electron transfer is fundamental to these redox-driven biogeochemical reactions, which dictate large-scale ecosystem responses[3]. Thus, the electron exchange capacities (EEC) of floodplain sediments—comprising electron-accepting (EAC) and electron-donating (EDC) capacities—are key redox parameters controlling their ecosystem function[3–5]. The concept of sediment EEC was introduced decades ago[6] and is generally considered to arise from the redox-active metastable phases present, including Fe/Mn minerals, natural organic matter (NOM), and sulfur-containing compounds[2]. However, direct and reliable measurements of EAC and EDC were limited until recent methodological advances[7,8], particularly mediated electrochemical reduction and oxidation[8,9]. Changes in EAC or EDC allow for quantifying the electron transfer direction and fluxes in redox processes. For instance, recent studies have revealed that EAC of particulate organic matter significantly suppresses methanogenesis in peatland via serving as a terminal electron acceptor[10] while sediment EDC governs oxidant consumption during in situ chemical oxidation of contaminated aquifers[7].

While the EEC of humic substances[9,11–13], Fe(III) (oxyhydr)oxides[14], and some types of Fe-bearing smectites[15] have been quantified, the EEC of whole sediments, especially floodplain sediments, remains poorly understood. Existing data are limited to a few studies of lake[5,16] and riparian sediments[7]. This knowledge gap arises from the chemical heterogeneity and the dynamic biogeochemical conditions of floodplain sediments. First, the presence of heterogeneous sediment components that can accept or donate electrons complicates the identification of bulk EEC sources. Floodplain sediments typically contain Fe-, Mn-, and S-bearing minerals resulting from natural weathering[17,18] and microbial processes[19]. These minerals exhibit no

[1]State Key Laboratory of Geohazard Prevention and Geoenvironment Protection, Chengdu University of Technology, Dongsanlu 1#, Erxianqiao, Chengdu, 610059 Sichuan, P.R. China. [2]State Key Laboratory of Environmental Criteria and Risk Assessment, Chinese Research Academy of Environmental Sciences, Beijing, 100012, P.R. China. [3]State Key Laboratory of Geomicrobiology and Environmental Changes, China University of Geosciences, Wuhan, Hubei, 430078, P.R. China. [4]Department of Geosciences, University of Tübingen, Tübingen, 72074, Germany. ✉e-mail: pushengyan13@cdut.edu.cn; wufengchang@vip.skleg.cn

to variable redox properties. For example, 24–41% of the total Fe in clay samples was redox-active in EEC measurements, while a significant portion of the mineral Fe was not[20]. Meanwhile, floodplain sediments also contain abundant solid organic matter (SOM) from terrigenous, microbial, and anthropogenic sources[21,22]. This SOM is expected to exhibit varying redox properties (i.e., EAC and EDC), as indicated by the broad range of EEC values (e.g., groundwater NOM[23]: 0.99–5.15 mmol e^- g C^{-1}; lake SOM[5]: 0.65 mmol e^- g C^{-1}) and their differing EAC/EDC ratios.

Second, geobatteries, such as Fe-bearing smectites[24], magnetite[25], and humic substances[26], further obscure the origin of sediment EEC. These phases cycle between electron donors (EDC) and acceptors (EAC) via microbial and/or chemical transformation of Fe(II)/Fe(III) pairs within minerals[24,25] or quinone/hydroquinone couples in NOM[26]. The role of a geobattery as either an EDC or EAC source is significantly influenced by redox fluctuations driven by groundwater table dynamics[2]. Third, SOM's contribution to sediment EDC and EAC is challenging to assess directly due to its heterogeneous composition. In comparison, quantification methods for the content and redox state of Fe/Mn minerals, which can be identified using well-established techniques, are more straightforward. Thus, SOM's contribution to sediment EEC remains speculative[4,5]. Overall, the EEC composition of floodplain sediments remains elusive. It is still unclear where electrons are stored and the chemical nature of EEC-related sites or molecules in bulk sediments. A molecular-level understanding of sediment EEC origin is essential for explaining variability in their biogeochemical reactivity.

In this study, we investigated the molecular composition of sediment EEC in floodplains from the upper and middle reaches of the Yangtze River, China. We quantified the EAC and EDC of 45 sediment samples, revealing that Fe-bearing minerals primarily contribute to sediment EAC, while SOM contributes more to EDC than EAC. We identified the redox-active Fe(III) and SOM compounds at the molecular level and established their correlations with sediment EAC and EDC, respectively. Finally, we demonstrate how anaerobic microbial respiration selectively converts Fe(III)-derived and SOM-derived EAC to EDC, discussing the implications for CH_4 suppression and green remediation of contaminated aquifers.

Results and discussion

Different contributions of Fe minerals and SOM to EAC and EDC of floodplain sediments

A total of 45 alluvial sediment samples were collected from the Chengdu Plain and Jianghan Plain in the upper and middle reaches of the Yangtze River (Fig. 1), representing diverse hydrological settings including farmland, riparian zones, lakeshores, wetlands, and a gasoline-contaminated aquifer. The sediments were sampled at depths of 0.4–10.2 m and below the groundwater table at 0.1–7.0 m. The sediment types primarily consisted of silt, silty loam, and sand, with particle size distributions of clay (<2 μm), silt (2–50 μm), and sand (50–2000 μm) ranging from 0.1–22.0%, 14.0–89.9%, and 0.2–86.0%, respectively (Supplementary Table S1). The heterogeneity of sediment particle size was also visually observed by SEM. For example, sediments from farmland and wetland contain more clay fraction, while riparian sediment contains a higher sand fraction (Supplementary Fig. S1). The contents of potential redox-active elements were as follows: 0.22–0.82 mmol g^{-1} for Fe (the sum of Fe(II) and Fe(III)), 0.31–1.65 mmol C g^{-1} for solid organic carbon (SOC), 0.036–0.18 mmol g^{-1} for N, ~0–0.095 mmol g^{-1} for S, and 0.007–0.036 mmol g^{-1} for Mn (Supplementary Table S2). The $Fe(II)/Fe_{total}$ ratios varied from 4.7% to 69.9%, indicating that these sediments originated from distinct redox environments or had varied redox histories. The measured EAC and EDC values ranged from 0.06 to 0.48 mmol e^- g^{-1} and ~0.0 to 0.078 mmol e^- g^{-1} (Supplementary Table S2), respectively, and their sum yielded EEC values between 0.066 and 0.50 mmol e^- g^{-1}. These values are similar to recently reported EAC (e.g., 0.03–0.16 mmol e^- g^{-1}) and EDC (e.g., 0.001–0.054 mmol e^- g^{-1}) for riparian aquifer sediments[7]. Both our findings and those of prior studies[7] suggest that the EEC of shallow aquifer sediments is predominantly comprised of EAC, which is in line with that for topsoils containing dissolved O_2[4] but contrast to the EDC-dominated EEC of clay rocks in the deep subsurface (e.g., 73–620 m)[20]. Thus, this EEC pattern results from long-term biogeochemical processes in floodplain shallow aquifers, with intermittent O_2 introduction caused by groundwater table fluctuation[27].

To investigate the influence of physical and chemical heterogeneity between sediment samples on EEC, we analyzed the relationship between measured EEC values and the physicochemical properties of the sediments. The EEC values were positively correlated with clay and silt content, but negatively correlated with sand content (all $p < 0.01$, Supplementary Fig. S1). The stronger correlation and steeper slope of the linear fit suggest that clay fractions predominantly influence sediment EEC. This correlation between sediment EEC and particle size reflects that the fine-grained fractions concentrate more redox-active Fe and the SOM phase[28].

Regarding the chemical properties, the measured EAC values showed a strong correlation with Fe(III) content ($R^2 = 0.707$, $p < 0.01$, Fig. 1a) while the SOC showed a moderate correlation ($R^2 = 0.282$, $p < 0.01$, Fig. 1b). These results indicate that Fe(III) is the primary contributor to the EAC of these sediments. Thus, sediments from the two floodplains exhibit similar EAC ranges because their Fe(III) contents span comparable ranges. Most EAC values of sediments were slightly below the 1:1 line of EAC: Fe(III) (Fig. 1a), suggesting that a small fraction of Fe(III) remains inactive for EAC quantification. SOM plays a secondary role in sediment EAC in this study, but can play a significant or even dominant role for the EAC in certain organic-rich environments, such as organic lake sediments (e.g., 11.0–27.4% SOC)[5] and peats (e.g., 33.6–42.7% SOC)[29]. Interestingly, the opposite pattern was observed for sediment EDC, with a much stronger correlation with the content of SOC ($R^2 = 0.733$, $p < 0.01$, Fig. 1e) or organic N ($R^2 = 0.458$, $p < 0.01$, Supplementary Fig. S3) compared to that of Fe(II) ($R^2 = 0.124$, $p < 0.05$, Fig. 1d). The investigated sediments from the Jianghan Plain have lower SOC contents than those from the Chengdu Plain and therefore exhibit lower EDC values. The significant role of SOM in EDC has also been observed in anoxic soils where SOM accumulates[4]. Although Fe(II) is often considered as the major contributor to sediment EDC[16], a large portion of the Fe(II) pool appears to be redox-inactive for EDC quantification, as values expressed as Fe(II) contents were much higher than EDC values (Fig. 1d). It was observed that a substantial fraction of Fe(II) in phyllosilicates could not donate electrons, which will be discussed in detail later. In contrast, S and Mn have a minimal contribution to EAC and EDC ($p > 0.05$, Supplementary Fig. S3) in these sediments due to their low contents (Supplementary Table S2). We then developed simple predictive models using both Fe and SOC contents to accurately reproduce the measured EAC and EDC data (Fig. 1c, f). The coefficients obtained from multiple linear regression further indicate the distinct roles of mineral Fe and SOM in EAC and EDC, pointing to the diverse reactivities of these two species under the same redox conditions.

Identification of reactive Fe(III) contributing to sediment EAC

The key Fe phases that are the potential sources of sediment EEC are identified by X-ray diffraction (XRD) analysis. Results showed that lepidocrocite and goethite are the predominant Fe(III) (oxyhydr)oxides in the sediments, together with abundant phyllosilicates including muscovite, biotite, chlorite, illite, and montmorillonite (Supplementary Fig. S4). These minerals are important Fe pools as indicated by the similar elemental distribution of Fe with O, Si, and Al across the imaged nanoscale regions (Supplementary Fig. S5). To quantify the reactive Fe(III) and explore their relationship with EAC, we employed two Fe extraction methods toward different Fe species. First, sequential extractions of selected sediments ($n = 13$) by sodium acetate (NaAc), hydroxylamine hydrochloride (HaHc), sodium dithionite–citrate–acetic acid (DCA), acidic ammonium oxalate (AAO), and H_2SO_4/HF target Fe species with increasing crystallinity. This method extracts Fe with increasing redox activity, following the order of adsorbed Fe > amorphous Fe > crystalline Fe in (oxyhydr)oxides > crystalline Fe in phyllosilicates[30]. Fe extraction results (Fig. 2a,

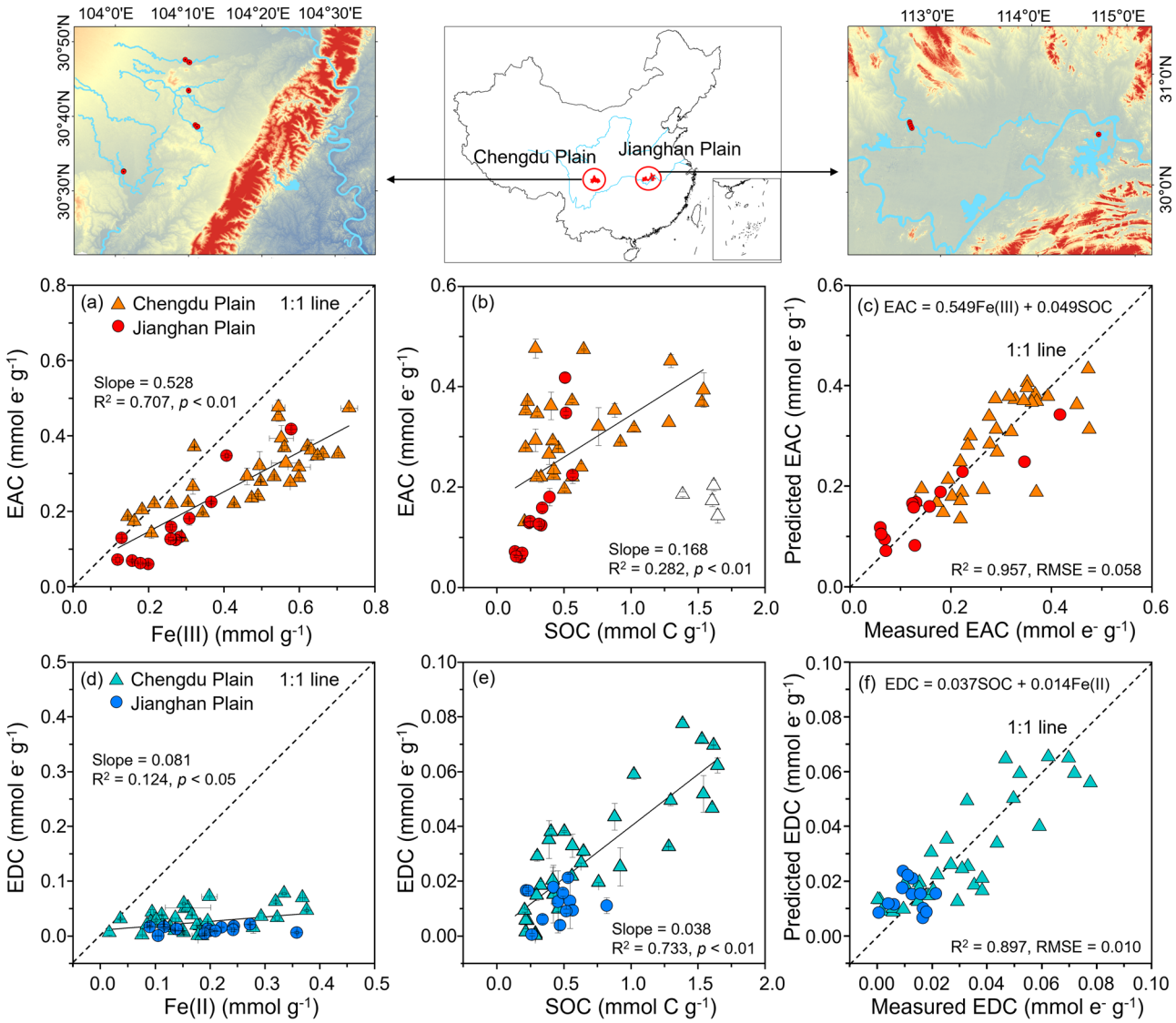

Fig. 1 | Correlations of sediment EEC with the contents of Fe and SOC. a Fe(III) vs EAC. **b** SOC vs EAC. **c** Prediction of sediment EAC. **d** Fe(II) vs EDC. **e** SOC vs EDC. **f** Prediction of sediment EDC. All data points from the 45 sediments were used for the linear fitting, except for the four data points (hollow circles) in panel (**b**). Error bars represent the standard deviations of two independent duplicate measurements (mean ± standard error).

Supplementary Table S3) also revealed the highest Fe concentrations in phyllosilicates (extracted by H_2SO_4/HF, 0.221 to 0.419 mmol g^{-1}), followed by DCA-extracted crystallized Fe (oxyhydr)oxides (0.003 to 0.173 mmol g^{-1}) and HaHc-extracted poorly crystallized Fe (oxyhydr)oxides (0.048 to 0.130 mmol g^{-1}). The sum of Fe species extracted by NaAc, HaHc, and DCA well correlates with sediment EAC ($R^2 = 0.497$, $p < 0.01$, Fig. 2b), indicating the dominant role of extractable Fe associated with Fe(III) (oxyhydr)oxides in EAC composition. It agrees with that Fe(III) (oxyhydr)oxides (e.g., ferrihydrite, goethite, and hematite) can accept electrons and can be fully electrochemically reduced for EAC quantification under the applied favorable thermodynamic conditions[14]. In contrast, the sum of Fe species extracted by AAO and H_2SO_4/HF showed poor correlation with sediment EAC ($R^2 = 0.220$, $p > 0.10$, Fig. 2b). However, because phyllosilicates host most of the Fe in the sediments and although not all of this Fe is redox-active and contributes to the EAC, it cannot be ruled out that some phyllosilicate Fe may still contributes to the sediment EAC.

Second, another sequential extraction distinguished the oxidation state of Fe. It revealed that exchangeable (extracted by $CaCl_2$) and surface-adsorbed Fe(III) (extracted by NaH_2PO_4) were extremely low (<0.012 mmol g^{-1}). Instead, the content of 6 M HCl extractable structural Fe(III) (Fe(III) (oxyhydr)oxides + a fraction of phyllosilicate Fe(III)) matches well with the measured sediment EAC (close to 1:1 line, $p < 0.01$, Fig. 2c). This suggests that 6 M HCl extractable reactive Fe(III), accounting for 40.2–100% of total Fe(III), are responsible for sediment EAC. As for Fe(II), phyllosilicates are the dominant hosts in these sediments. The content of other possible Fe(II)-bearing phase such as pyrite (FeS_2) and mackinawite (FeS) is extremely low as reflected by XRD and S element contents (Supplementary Fig. S4, Table S2). Surface-associated Fe(II) in phyllosilicates is much more reactive in donating electrons than interior structural Fe(II)[31,32], but their contents are low for these sediments (0.001–0.017 mmol g^{-1}, Supplementary Table S4). This is also indicated by the XPS-identified low ratios of $Fe(II)/Fe_{total}$ (14.9–35.3%, Supplementary Fig. S6) at sediment surfaces. Sediment EDC correlates poorly with the content of surface-adsorbed Fe(II) and/or HCl-extracted structural Fe(II) (Supplementary Fig. S7), indicating the contribution of phyllosilicate Fe(II) to sediment EDC is either not linear or not significant.

The higher Fe content measured in sediments than the EAC or EDC values was attributed to the fractions of low or non-redox-active Fe(III) and Fe(II) in phyllosilicates. Previous studies found that Fe in 2:1 smectites (e.g., SWa-1 and SWy-1) is all redox-active[15] while only 11–22% Fe in illite is

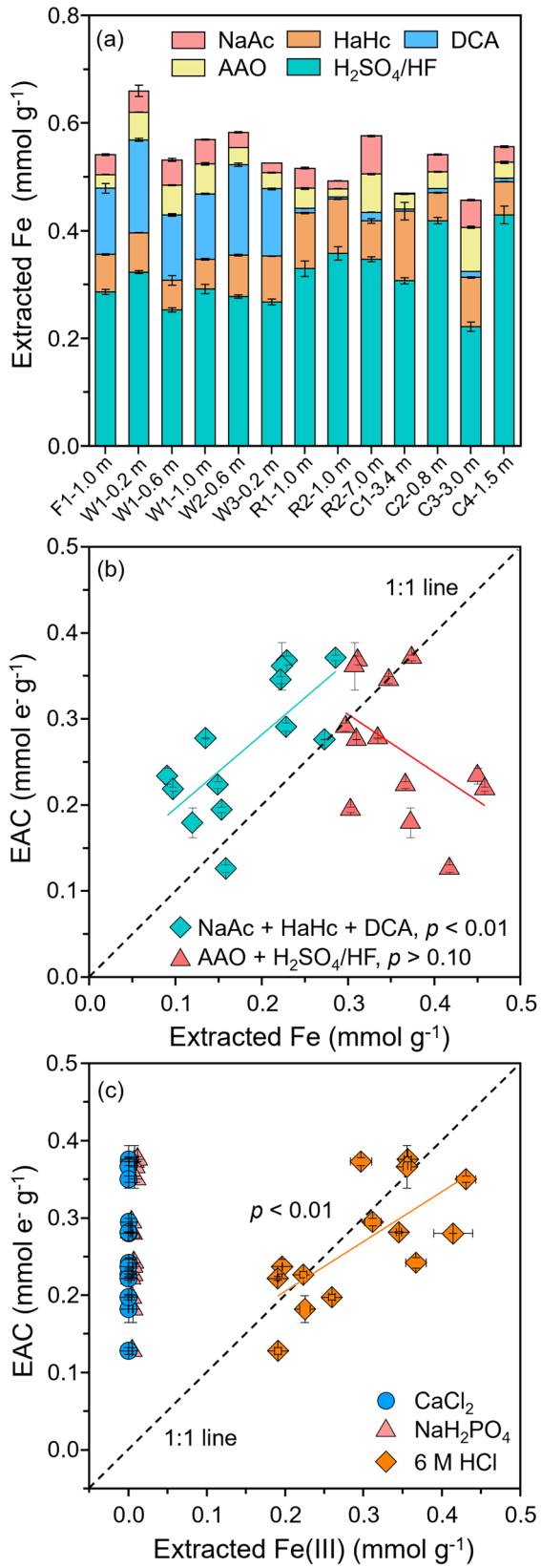

Fig. 2 | Correlations between different Fe(III) species and sediment EAC. **a** Distribution of Fe species in selected sediments ($n = 13$); **b** Relationship between extracted Fe content and sediment EAC; **c** Relationship between extracted Fe(III) content and sediment EAC. Error bars represent the standard deviations of two independent duplicate measurements (mean ± standard error).

redox-active[33]. The redox activities of Fe associated with phyllosilicates are significantly influenced by the interlayer expandability, which determines the electron exchange of interior Fe through the redox-inert siloxane plane. Phyllosilicates such as illite, biotite, and chlorite are typically unexpandable due to the large layer charge, exhibiting weak to no ability of electron donating or accepting[34,35]. In addition to expandability, the coordination and arrangement of structural Fe in phyllosilicates also significantly influence its redox activity. For example, biotite and chlorite typically contain high contents of trioctahedral Fe(II) that are difficult to oxidize, due to the constraints of charge balances[36]. Thus, the contribution of phyllosilicate Fe to EEC exhibits no linear correlation with Fe content but should be attributed to the reactive Fe associated with redox-active phyllosilicates (especially expandable smectite).

Role of molecular redox properties of SOM in the constitution of sediment EDC

To directly assess the contribution of SOM to sediment EEC, we extracted water-extractable organic matter (WEOM), fulvic acids (FA), and humic acids (HA) from selected sediments ($n = 9$, Supplementary Table S5) under anoxic conditions and quantified their EEC. The EEC values ranged from 0.83 to 6.01 mmol e^- g C^{-1} for WEOM, 1.22–7.83 mmol e^- g C^{-1} for FA, and 1.99–12.0 mmol e^- g C^{-1} for HA (Supplementary Table S6), comparable to values reported for IHSS humic substances[13], dissolved organic matter (DOM) in groundwater [23] and lake[37], and extracted soil organic matter[38]. Among the three SOM components, EDC values followed the order of HA (3.91 ± 1.75 mmol e^- g C^{-1}) > FA (2.32 ± 1.51 mmol e^- g C^{-1}) > WEOM (1.59 ± 1.58 mmol e^- g C^{-1}) (Fig. 3b). This sequence can be attributed to differences in the abundance of redox-active moieties, as reflected by their respective EEC values. Moreover, all HA samples exhibited EDC values greater than their corresponding EAC, with EDC/EAC ratios ranging from 1.1 to 22.7. In contrast, 33.3% of FA and 55.6% of WEOM samples showed EAC values exceeding EDC (Fig. 3a). These findings suggest that FA and WEOM are more prone to oxidation by microbes or dissolved oxidants (e.g., O_2)[27,39], than HA in the groundwater fluctuation zone, likely due to their higher solubility and the associated SOM-to-DOM transformation. Consequently, HA exhibits the highest EDC among the three SOM fractions, reflecting both its intrinsic redox properties and the influence of in situ redox conditions.

A significant positive correlation ($R^2 = 0.570$, $p < 0.05$; Fig. 3c) was observed between the sum of EDC values from the three extracted SOM fractions and the bulk sediment EDC, supporting the important contribution of SOM to sediment EDC. These extractable fractions accounted for 13.0–63.5% of total sediment SOM mass (Supplementary Table S5) and contributed 5.2–31.7% of the measured sediment EDC. The remaining unextractable SOM, largely composed of humin[40], was not quantified directly. Using reported EEC values for terrigenous humin (0.544 mmol e^- g C^{-1} for EDC and 0.628 mmol e^- g C^{-1} for EAC)[41] to represent this fraction, the total contribution of SOM to sediment EDC was estimated to range from 12.9–61.2%, leaving the estimated contribution of structural Fe(II) associated with redox-active phyllosilicates (e.g., expandable smectites) ranging from 38.8% to 87.1%. In contrast, the estimated contribution of SOM to sediment EAC was notably low (2.1–7.9%), while that of Fe(III) could be 92.1–97.9%.

The bulk optical properties of WEOM, FA, and HA were analyzed to infer their redox characteristics related to EDC. Among the three fractions, WEOM exhibited the lowest $SUVA_{254}$ and humification index (HIX) values (Fig. 3d, e), indicating its relatively low aromaticity and humification degree. Previous studies have shown that higher $SUVA_{254}$ or aromaticity in environmentally derived organic matter is often, but not always[42], associated with higher EDC and lower EAC[13,43]. This relationship explains why WEOM has the lowest EDC but largest EAC among the three SOM fractions (Supplementary Table S6). The biological index (BIX) and fluorescence index (FI) values suggest that WEOM and FA are derived from a mixture of microbial and terrestrial sources, whereas HA is predominantly

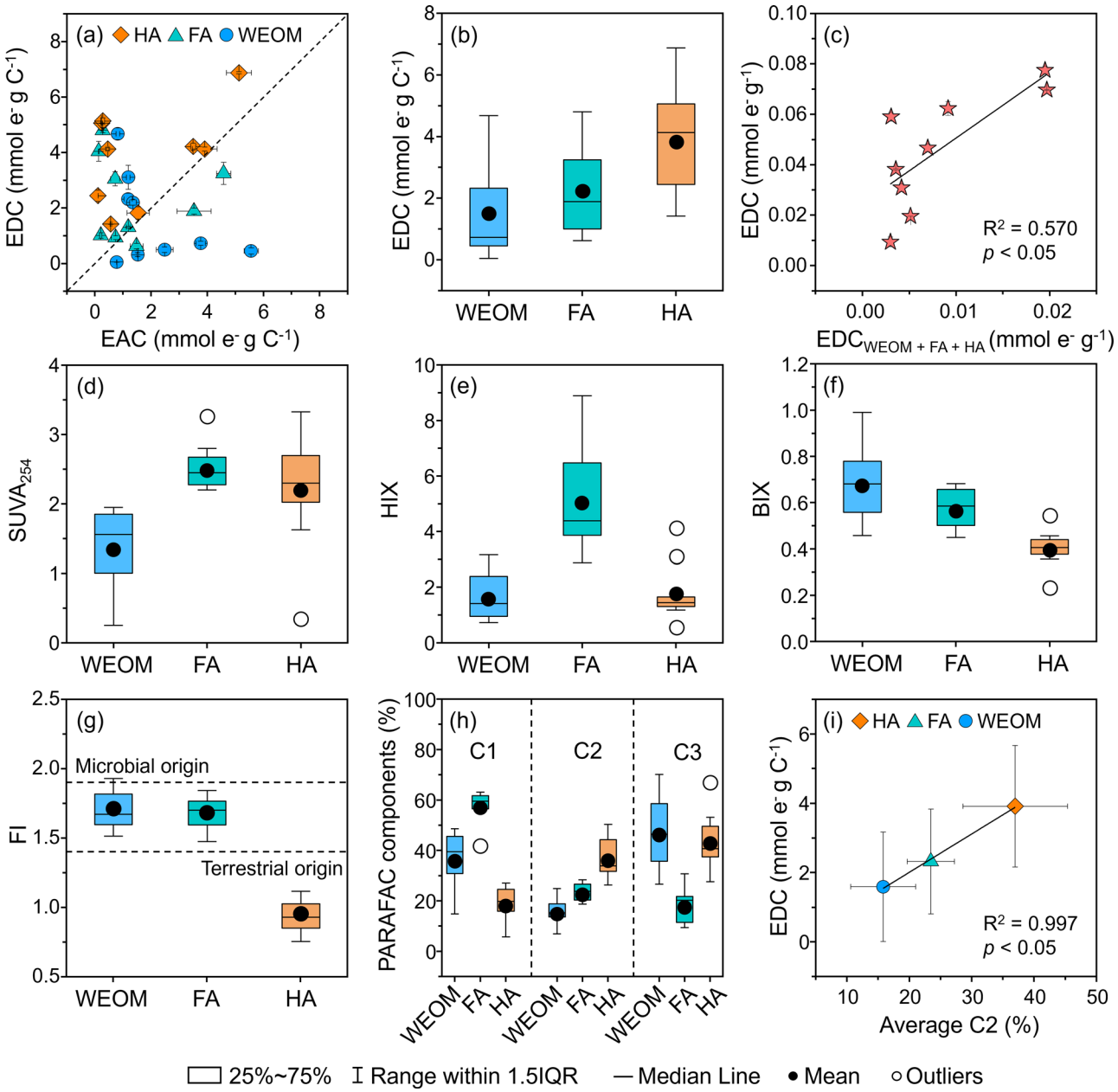

Fig. 3 | Optical properties of SOM fractions associated with EDC. a EDC and EAC values of HA, FA, and WEOM. **b** Average values of the three SOM fractions. **c** Sum of EDC from the three SOM fractions versus sediment EDC. **d** $SUVA_{254}$ values. **e** HIX values. **f** BIX values. **g** FI values. **h** Relative abundance of PARAFAC components in the three SOM fractions. **i** Correlation between EDC and C2 content. Error bars represent the standard deviations (mean ± standard deviation) in (**a**, **c**, **i**). The empty circles, lines within each box, and the lower and upper edges of the boxes represent the means, medians, and the 25th and 75th percentiles, respectively. The whiskers indicate the most extreme values within 1.5 times the interquartile range.

of terrestrial origin (Fig. 3f, g). According to the "enzymic latch" hypothesis[44], enzymatic oxidation of phenolic moieties in DOM—particularly in the presence of dissolved oxygen—can irreversibly lower EDC values[43]. Therefore, the lower EDC of WEOM and FA may result from microbial transformation processes, which tend to diminish redox-active moieties, in contrast to the more recalcitrant and redox-active terrestrial components in HA. A three-component parallel factor analysis (PARAFAC, Supplementary Fig. S8) model further supports this interpretation: HA contained the highest proportion of terrestrial humic-like components (C2: 37.0%), compared to FA (23.5%) and WEOM (15.9%) (Fig. 3h and Supplementary Fig. S8). Notably, the average EDC values of the three SOM fractions were linearly correlated with their C2 contents ($R^2 = 0.997$, $p < 0.05$; Fig. 3i), highlighting terrestrial humic-like substances as the dominant contributors to EDC of SOM.

To gain molecular-level insights into the contribution of SOM components to EDC, we analyzed the molecular compositions of WEOM, FA, and HA extracted from two representative sediment samples using electrospray ionization Fourier-transform ion cyclotron resonance mass spectrometry (ESI-FT-ICR-MS). We first examined the relationship between SOM EDC and the redox state of organic molecules. Results revealed that SOM fractions with higher EDC values comprised molecules in more reduced states, as evidenced by significant negative correlations between EDC and both the average double bond equivalent (DBE) and nominal oxidation state of carbon (NOSC) (Fig. 4a, b). Since microbial degradation of organic molecules with higher NOSC is more thermodynamically favorable under reducing conditions[45], these findings suggest that WEOM and FA are more readily oxidized by microbes than HA, resulting in the loss of EDC. Van Krevelen diagrams indicated that the molecular compositions

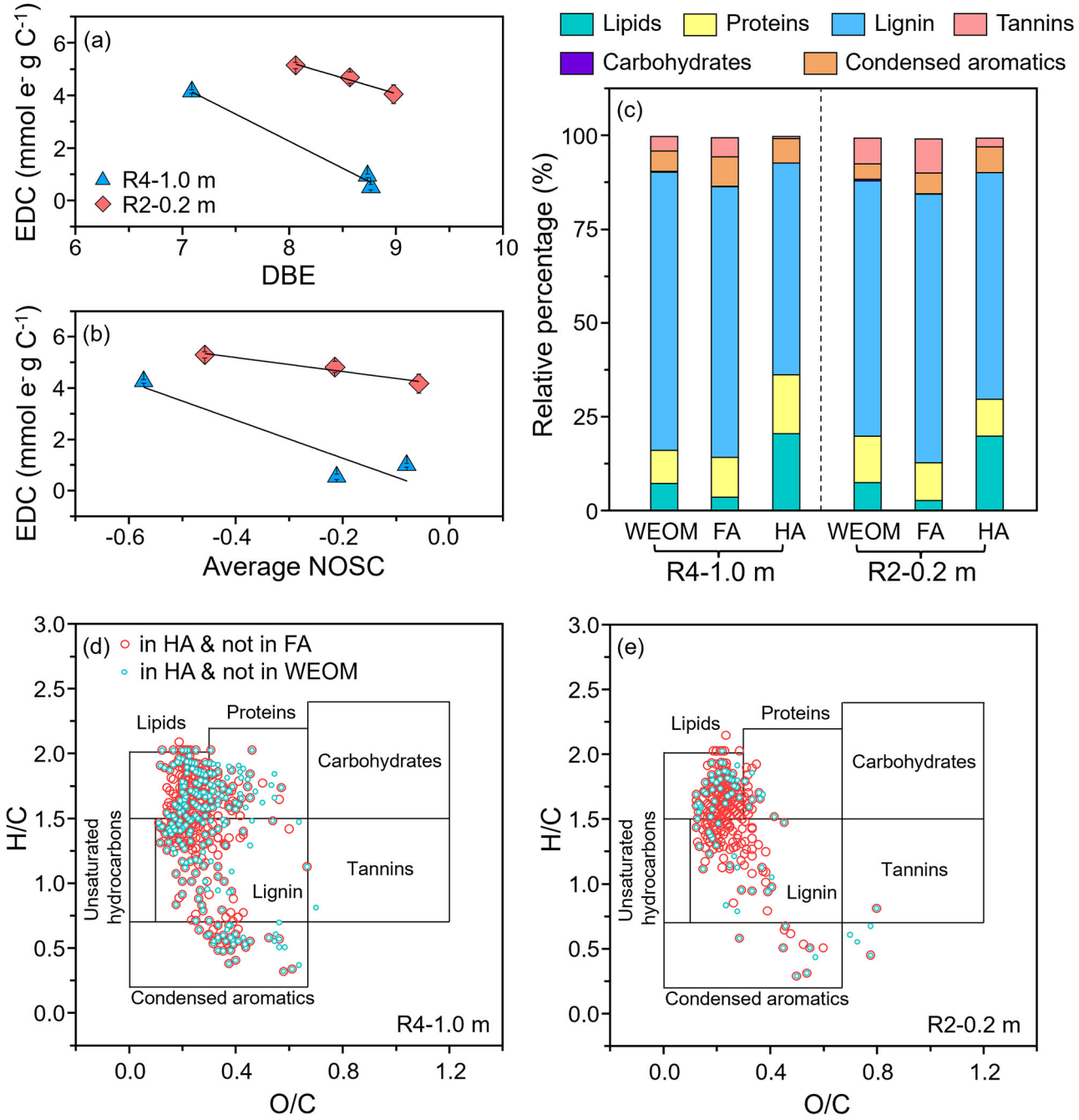

Fig. 4 | Molecular properties of SOM fractions associated with EDC. a Correlation between EDC values of SOM fractions and average DBE. **b** Correlation between EDC values of SOM fractions and average NOSC. **c** Abundance-weighted percentages of different molecular components in the three SOM fractions. **d**, **e** Unique molecules present in HA but absent in FA and WEOM.

of HA, FA, and WEOM were dominated by lignin-like compounds (56.4–74.2%), with additional contributions from lipids, proteins, condensed aromatics, and tannins (Fig. 4c, Supplementary Fig. S9). Generally, lipids and proteins were preferentially biodegradable in sediments[46] while lignin-like and aromatic compounds are recalcitrant and related to EEC[23]. Since HA has the largest EDC, we identified compounds that were uniquely present in HA but absent from WEOM and FA. Results revealed that the lignin-like compounds unique in HA from sediment R4–1.0 m has a twice as high number of formulas than those from sediment R2–0.2 m (Fig. 4d, f), corresponding with a larger EDC difference between HA and FA/WEOM in the R4–1.0 m sample (Fig. 4a). These unique lignin-like compounds from two sediments are CHO-dominated and characterized by lower average O/C ratios (0.24–0.26 vs 0.38–0.47), higher H/C ratios (1.27–1.29 vs 1.08–1.18), lower DBE (8.33–8.92 vs 8.35–9.59) and lower NOSC (−0.80 to −0.70 vs −0.38 to −0.04) than the bulk lignins in three SOM fractions (Supplementary Table S7). These molecular features indicated that these compounds contain more phenolic moieties (i.e., electron-donating groups) and are in a more reduced redox state. Based on the relationships of EDC with DBE and NOSC, these identified molecules greatly contribute to the SOM EDC.

Selective transformation of EAC from Fe(III) and SOM into EDC during microbial reduction

Since microbial electron transfer plays a critical role in regulating the redox state of mineral Fe and SOM, we explored the composition-dependent selectivity of sediment EEC fractions during microbial reduction by Fe(III)-

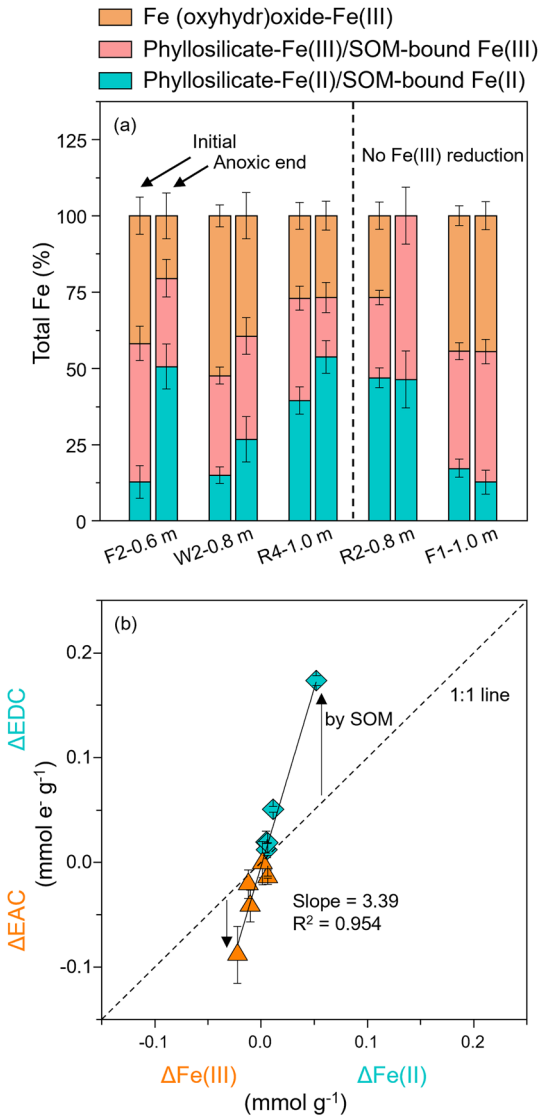

Fig. 5 | Contributions of mineral Fe and SOM to EEC variations during microbial reduction of sediments. a Proportions of Fe(II)/Fe(III) in sediments before and after microbial reduction. **b** Correlations between changes in Fe(II) and Fe(III) contents and variations in EDC and EAC. The arrows in panel **b** indicate the contribution of SOM to ΔEDC and ΔEAC. **c** The conceptual diagram depicting the selective transformation of EAC into EDC by microbes. All sediments were pre-oxidized with O_2 for 24 h. Sediment Fe was extracted using 6 M HCl to represent the redox-active fraction. Error bars represent the standard deviations of two independent duplicate measurements (mean ± standard deviation).

reducing microbes (Shewanella oneidensis MR-1). To improve the reducibility of sediments, they were pre-oxidized by O_2 (99.999%) after 24-h aeration. Mössbauer spectra revealed that there are still large fractions of phyllosilicate Fe(II) ($Fe(II)_{phyllosilicates/SOM}/Fe_{phyllosilicates/SOM,\ total}$: 21.9–64.0%) in sediments that showed no reactivity toward O_2 during 24-h pre-oxidation (Fig. 5a, Supplementary Fig. S10 and Table S8). This confirms our abovementioned conclusion that phyllosilicates in sediments contain a considerable percentage of non-redox-active structural Fe(II) (and Fe(III)) that makes no contribution to sediment EEC. After 5d-microbial reduction, the increase in sediment EDC is comparable to the decrease in EAC, indicating the microbial conversion of EAC into EDC (Fig. 5b). Meanwhile, the Fe(III) contents in sediments F2-0.6 m, W2-0.8 m, and R4-1.0 m decreased accompanied with equal increase in Fe(II) contents, which account for 11.8–37.9% of Fe_{total} (Fig. 5a). In contrast to these three sediments, no microbial reduction of Fe(III) was observed in R2-0.8 m and F1-1.0 m (Fig. 5a). Fe extraction results indicated that the variations of EDC and EAC correlates with the changes of 6 M HCl-extracted Fe(II) and Fe(III) contents ($R^2 = 0.954$, $p < 0.005$, Fig. 5b and Supplementary Fig. S11), giving a slope of 3.39. This slope is much larger than a theoretical value of 1 if mineral Fe dominates the microbial transformation of sediment EAC to EDC, suggesting an additional important role of SOM. The significant contribution of SOM serving as the terminal electron acceptor can be seen for R2-0.8 m and F1-1.0 m in which no reduction of Fe(III) to Fe(II) occurs (Fig. 5a) but the variations in EDC and EAC are pronounced (Supplementary Fig. S11). Note that the decrease in Fe (oxyhydr)oxide–Fe(III) and the increase in phyllosilicate-Fe(III)/SOM-bound Fe(III) for sediment R2-0.8 m may indicate that Fe(III) (oxyhydr)oxides were dissolved by chemical or microbial processes, and the released Fe(III) subsequently adsorbed onto SOM or phyllosilicate surfaces. These results suggest that SOM also makes a considerable contribution to microbially available EAC, although its bulk EAC is smaller than that of sediment Fe(III). Quinone moieties (C=O, Supplementary Fig. S12) in lignin-like compounds and condensed aromatics are the likely dominant electron-accepting sites in SOM.

The Fe(III) utilized by Fe(III)-reducing microbes as the terminal electron acceptors can be either solo Fe (oxyhydr)oxide-Fe(III) (W2-0.8 m) or solo phyllosilicates/SOM-Fe(III) (R4-1.0 m) or both (F2-0.6 m) (Fig. 5a). Although Fe (oxyhydr)oxides-Fe(III) is usually considered more readily to be microbially reduced than phyllosilicates-Fe(III), their reduction likely depends on the preferential contact between Fe(III)-reducing microbes and the Fe(III) mineral exposed at sediment surfaces[47,48]. Similarly, the dependence of electron acceptor selection for Fe(III) or SOM can also be kinetically constrained by the preferential contact with Fe(III) sites and SOM moieties. This hypothesis can be supported by that Fe(III)-reducing microbes tend to preferentially utilize SOM-dominated EAC for sediments with high $SOC/Fe(III)_{6M\ HCl}$ ratios (e.g., >6.6 for R2-0.8 m and F1-1.0 m), while utilize EAC from both Fe(III) and SOM for sediments with low $SOC/Fe(III)_{6M\ HCl}$ ratios (e.g., 1.5–3.6 for R2-0.8 m and F1-1.0 m).

In addition to physical contact, the redox potentials of sediment compositions could also influence the microbial selection for different sources of EAC. The reduction potentials (E_h) of MtrC and OmcA, the outer-membrane decaheme *c*-Cyts of *Shewanella oneidensis* MR-1 functioning as terminal reductases, are reported to range from −0.400 to 0.100 V and from −0.320 to −0.100 V, respectively[49]. The E_h values (vs SHE) of Fe-bearing minerals are estimated to be +0.106 V for ferrihydrite, −0.061 V for lepidocrocite, and −0.110 V for goethite[50]. It is possible that phyllosilicates with high $Fe(II)/Fe_{total}$ (e.g., 64.1% for R2-0.8 m) have even lower redox potentials and thus is thermodynamically unfavorable to be reduced by *Shewanella oneidensis* MR-1. In contrast, air-oxidized HA is reported to contain electron-accepting moieties with higher reduction potentials (e.g., E_h: from 0 to +0.1 V) and hence more readily accept electrons from

Shewanella oneidensis MR-1[26]. Together, our results demonstrated that the microbial selection of Fe(III)-sourced and SOM-sourced EAC can be regulated by both kinetic and thermodynamic constraints (Fig. 5c). As a result, Fe(II)-sourced and SOM-sourced EDC were generated.

Implications for methanogenesis suppression and green remediation

Identification of the sediment EAC origin has important implications for greenhouse gas emissions. Both mineral-associated Fe(III) (in Fe(III) (oxyhydr)oxides[51] and phyllosilicates[52]) and SOM[53] can serve as terminal electron acceptors for anaerobic respiration. Anaerobic respiration utilizing these microbially available EAC components is more thermodynamically favorable than methanogenesis[10], thus suppressing CH_4 formation (Fig. 5c). Methanogenic conditions can be established only after the available EAC are depleted[10]. In this study, the ΔEAC values during anoxic incubation represent the microbially available EAC pools. We estimated that microbial utilization of EAC pools derived from Fe(III) and SOM in sediments may suppress CH_4 emissions by approximately 2.15×10^5–1.89×10^7 mol CH_4 km^{-2} yr^{-1}, assuming an average annual water table fluctuation of 2.2 m (Supplementary Information Text S2). This suppression potential is substantial when compared to reported annual net CH_4 fluxes of 2.9×10^4 to 1.3×10^6 mol CH_4 km^{-2} yr^{-1} for the Chengdu Plain[54] and 1.4×10^5 to 1.9×10^7 mol CH_4 km^{-2} yr^{-1} for the Jianghan Plain[55]. Based on a global floodplain area of 15 million km^2[21], the microbially available EAC of sediments could potentially lower a significant amount of CH_4 formation by 51.6–4536 Tg C yr^{-1} when compared to the CH_4 emission in the global terrestrial biosphere (325 ± 39 Tg C yr^{-1})[56]. This estimation highlights the importance of floodplain sediment EAC in mitigating the global flux of strong greenhouse gas CH_4. In addition, sediment EAC may further lower CH_4 concentrations by accepting electrons from anaerobic oxidation of CH_4[57]. Therefore, the suppression of CH_4 production depends not on the bulk EAC but on the microbially utilizable fraction, which is controlled by EAC composition.

Deciphering the composition of sediment EEC also offers valuable insights for guiding in situ chemical oxidation (ISCO) during contamination remediation. Traditional ISCO commonly involves injecting excess oxidants (e.g., persulfate) into contaminated aquifers due to insufficient information on the oxidant consumption capacity of aquifer sediments[58]. Instead, low-oxidant-consumption remediation can be achieved by precisely characterizing the redox capacity of contaminated aquifers. Our recent studies have established the correlation of initial sediment EDC with the consumption of persulfate ($S_2O_8^{2-} + 2EDC \rightarrow 2SO_4^{2-} + 2EAC$)[7]. While sedimentary Fe(II) has been widely recognized as the dominant activator of persulfate[59], our current results suggest that the role of SOM should not be overlooked, as it constitutes a significant portion of sediment EDC. In addition, Fe(III) (oxyhydr)oxides in aquifer materials are capable of activating persulfate, albeit at substantially lower reaction rates than mineral-associated Fe(II), resulting in half-lives on the order of months[60]. Based on these findings, we propose that sediment EDC derived from SOM and Fe(II) controls remediation performance over short timescales (hours to days), whereas sediment EAC associated with Fe(III) (oxyhydr)oxides controls the performance of long-term remediation (weeks to months). Thus, a survey of aquifer sediment EEC and its origin can guide the time, location, and dosage of oxidant injection for low-oxidant-consumption remediation.

Methods

Sample collection and preparation

Sediment samples ($n = 45$) were collected from March to June 2024 from the Chengdu Plain and the Jianghan Plain along the Yangtze River (Supplementary Table S1). Samples were obtained from depths of 0.1–7.0 m below the groundwater table, corresponding to unconfined aquifers, using a handheld auger or shovel. Immediately after collection, sediments were vacuum-sealed on site and transported to the laboratory, where they were stored at −20 °C in the dark. Prior to analysis, samples were freeze-dried by freezing at −60 °C for 6 h followed by vacuum drying for 24 h. The dried sediments were then processed in an anoxic glovebox (99.999% Ar, Mikrouna Co., Ltd., China), where they were ground, sieved through a 220-mesh (75 μm) sieve, and suspended at 10 g L^{-1} in brown glass bottles. Aliquots of these suspensions were used to determine the EEC via mediated electrochemical analysis.

EDC and EAC measurements

The EDC and EAC of sediment samples were quantified via mediated electrochemical analysis in reduction (MER) and oxidation (MEO) modes, respectively[4,5,8]. Measurements were conducted at pH 7.0 in a solution containing 0.1 M KCl and 0.01 M MOPS buffer, using a vitreous carbon working electrode, an Ag/AgCl reference electrode, and a platinum wire counter electrode. All analyses were performed in an anaerobic glovebox using a CHI1000C electrochemical workstation (Shanghai CH Instruments, China). ABTS (2,2′-azino-bis(3-ethylbenzothiazoline-6-sulfonic acid)) and EtV (ethyl viologen) were used as electron-transfer mediators for MEO and MER, respectively, each at a final concentration of 250 μM. Electrodes were pre-equilibrated at the target potentials ($E_h = +0.70$ V vs. SHE for MEO; $E_h = -0.45$ V vs. SHE for MER), followed by addition of the mediator to generate oxidative or reductive background currents. After stabilization, sediment samples were added to the cell at a final concentration of 125 mg L^{-1}. Electron exchange between the sediment and the electrode, mediated via the redox shuttles, was quantified by integrating the resulting current over time. All the measurements were conducted at least in duplicate.

Chemical analysis of sediments

The contents of redox-active elements, including C/N, S, Mn, and Fe, were determined. SOC content was measured using a 902T C–S analyzer (Beijing Wanliandaxinke Instruments Co., China). Total N and S contents were analyzed with an elemental analyzer (Elementar UNICUBE, Germany). The total organic carbon (TOC) of extracted SOM fractions was determined employing a TOC analyzer (Shimadzu, TOC-L CPH, Japan). Mn content was determined by inductively coupled plasma mass spectrometry (ICP-MS; Agilent 5110, USA) after microwave-assisted acid digestion of 100 mg of sediment. Total Fe(II) and Fe(III) were quantified using the 1,10-o-phenanthroline analytical method at 510 nm (UV-2600i spectrophotometer, Shimadzu)[61] following the extraction of sediment with H_2SO_4/HF. To characterize Fe speciation, two parallel sequential extraction schemes were conducted. In the first scheme, sediments were sequentially extracted with sodium acetate (NaAc), hydroxylamine hydrochloride (HaHc), sodium dithionite–citrate–acetic acid (DCA), acidic ammonium oxalate (AAO), and H_2SO_4/HF, targeting Fe bound to carbonates, poorly crystalline Fe(III) (oxyhydr)oxides, crystalline Fe(III) (oxyhydr)oxides, magnetite, and silicates, respectively[36]. In the second scheme, 1 M $CaCl_2$, 1 M NaH_2PO_4, and 6 M HCl were used sequentially to extract ion-exchangeable, surface-adsorbed, and structural Fe, respectively[36].

Sediment characterization

The mineralogical composition of the sediments was analyzed using X-ray diffraction (XRD; D8 Advance, Bruker) at 40 kV and 40 mA, with a scanning range of 5–90° 2θ, a step size of 0.01°, and a step time of 0.05 s. Surface redox properties of Fe and SOM were characterized by X-ray photoelectron spectroscopy (XPS; ESCALAB 250Xi, Thermo Scientific) using a monochromatic Al Kα X-ray source ($h\nu = 1486.6$ eV). Binding energies were calibrated to the C 1s peak at 284.8 eV. Morphological features and elemental distributions were examined by scanning electron microscopy (SEM) coupled with energy-dispersive X-ray spectroscopy (EDS; Sigma 300, Zeiss) operated at an accelerating voltage of 3 kV. Sediment particle size distributions were measured using the Mastersizer instrument (Malvern).

Mössbauer spectroscopy

Mössbauer spectra were collected in transmission geometry using a constant-acceleration spectrometer (Wissel MS-500, Germany) equipped with a ^{57}Co(Rh) source (25 mCi). Absorbers containing dry sediment

powder were mounted in a cryostat (Air Products, USA) under vacuum (2×10^{-4} Pa) maintained by a molecular pump. Velocity calibration was performed using an α-Fe foil at 13 K over a velocity range of −8 to 8 mm s^{-1}. Spectral fitting was conducted with Recoil software (Ottawa, Canada) using Lorentzian line shapes and a multi-site analysis model.

3D-EEM and ESI-FT-ICR-MS

WEOM, FA, and HA were extracted from sediments under anoxic conditions following previously established protocols[40]. The fluorescence characteristics of extracted SOM fractions were analyzed using three-dimensional excitation–emission matrix (3D-EEM) fluorescence spectroscopy (Hitachi F-4700), with excitation wavelengths ranging from 200 to 400 nm and emission wavelengths from 220 to 600 nm.

The molecular composition of extracted WEOM, FA, and HA was elucidated using ESI-FT-ICR MS[62]. Specifically, analysis was performed utilizing a 9.4 T Bruker Apex Ultra FT-ICR-MS coupled with negative-ion Apollo II electrospray ionization (ESI) at a rate of 250 mL h^{-1}. The operating conditions were as follows: a spray shield voltage of 2.7 kV, a capillary column introduced voltage of 4.5 kV, and a capillary column end voltage of 2320 V. The ion transformation parameter for the quadrupole (Q1) was optimized at m/z 200, and the mass range was m/z 150 to 800 Da. Each mass spectrum was acquired by conducting 128 single scans with 4 M words to enhance the signal-to-noise (S/N) ratio. Mass peaks exhibiting an S/N greater than 6 were exported for data analysis utilizing in-house software. MF assignments were based on the elemental compositions of $^{12}C_{1-60}$, $^{1}H_{1-120}$, $^{14}N_{0-3}$, $^{16}O_{0-30}$, and $^{32}S_{0-1}$. All assigned formulas had to meet the following basic chemical criteria: (i) the number of H atoms was at least 1/3 that of C atoms, not exceeding $2C + N + 2$; (ii) the sum of H and N atoms was even (the nitrogen rule); and (iii) the number of N or O atoms did not exceed the number of C atoms. The molecular parameters of SOM fractions were calculated and provided in Supplementary Information Text S1.

Sediment incubation

To assess the selection of EAC for microbial reduction, we incubated sediments with Fe(III)-reducing microbes (*Shewanella oneidensis* MR-1) under anoxic conditions. Four grams of sediments were mixed with 1×10^9 CFU mL^{-1} MR-1 suspensions in 80 mL of oxygen-free ultrapure water. The suspensions were purged with N_2 (99.999%) for 30 min to remove dissolved oxygen and transferred into the anoxic glovebox. Sediment suspensions were slowly stirred and incubated at room temperature (25 ± 2 °C) for 5 days. Then, sediment samples were taken out by 1 mL for Fe measurement, by 4 mL for EEC analysis, and 4.5 mL for Mössbauer spectroscopic characterization. Note that the redox-reactive Fe in these sediments was extracted using 6 M HCl for 12 h, as this fraction contributes to the sediment EEC (Fig. 2).

Data availability

All data generated in this study are included in this published article and its Supplementary Materials. Source data are provided with this paper.

Received: 15 September 2025; Accepted: 4 February 2026;
Published online: 21 February 2026

References

1. Rajib, A. et al. Human alterations of the global floodplains 1992–2019. *Sci. Data* **10**, 499 (2023).
2. Peiffer, S. et al. A biogeochemical-hydrological framework for the role of redox-active compounds in aquatic systems. *Nat. Geosci.* **14**, 264–272 (2021).
3. Zhang, Y. et al. Directional long-distance electron transfer from reduced to oxidized zones in the subsurface. *Nat. Commun.* **15**, 6576 (2024).
4. Aeppli, M., Thompson, A., Dewey, C. & Fendorf, S. Redox properties of solid phase electron acceptors affect anaerobic microbial respiration under oxygen-limited conditions in floodplain soils. *Environ. Sci. Technol.* **56**, 17462–17470 (2022).
5. Lau, M. P., Sander, M., Gelbrecht, J. & Hupfer, M. Solid phases as important electron acceptors in freshwater organic sediments. *Biogeochemistry* **123**, 49–61 (2015).
6. Heron, G., Christensen, T. H. & Tjell, J. C. Oxidation capacity of aquifer sediments. *Environ. Sci. Technol.* **28**, 153–158 (1994).
7. Lu, Y. et al. Accurate and simple determination of sediment redox capacity by a modified chemical probe method: implications to contaminant remediation. *Water Res* **284**, 124014 (2025).
8. Sander, M., Hofstetter, T. B. & Gorski, C. A. Electrochemical analyses of redox-active iron minerals: a review of nonmediated and mediated approaches. *Environ. Sci. Technol.* **49**, 5862–5878 (2015).
9. Aeschbacher, M., Sander, M. & Schwarzenbach, R. P. Novel electrochemical approach to assess the redox properties of humic substances. *Environ. Sci. Technol.* **44**, 87–93 (2010).
10. Gao, C. Y., Sander, M., Agethen, S. & Knorr, K. H. Electron accepting capacity of dissolved and particulate organic matter control CO_2 and CH_4 formation in peat soils. *Geochim. Cosmochim. Acta* **245**, 266–277 (2019).
11. Liu, Y. et al. Asymmetrical changes of electron-donating and electron-accepting capacities of natural organic matter during its interaction with Fe oxyhydroxides. *Chem. Geol.* **661**, 122189 (2024).
12. Yang, P. et al. Loss and increase of the electron exchange capacity of natural organic matter during its reduction and reoxidation: The role of quinone and nonquinone moieties. *Environ. Sci. Technol.* **56**, 6744–6753 (2022).
13. Aeschbacher, M., Graf, C., Schwarzenbach, R. P. & Sander, M. Antioxidant properties of humic substances. *Environ. Sci. Technol.* **46**, 4916–4925 (2012).
14. Aeppli, M., Voegelin, A., Gorski, C. A., Hofstetter, T. B. & Sander, M. Mediated electrochemical reduction of iron (oxyhydr-)oxides under defined thermodynamic boundary conditions. *Environ. Sci. Technol.* **52**, 560–570 (2018).
15. Gorski, C. A. et al. Redox properties of structural Fe in clay minerals. 1. Electrochemical quantification of electron-donating and -accepting capacities of smectites. *Environ. Sci. Technol.* **46**, 9360–9368 (2012).
16. Aeppli, M., Schladow, G., Lezama Pacheco, J. S. & Fendorf, S. Iron reduction in profundal sediments of ultraoligotrophic Lake Tahoe under oxygen-limited conditions. *Environ. Sci. Technol.* **57**, 1529–1537 (2023).
17. Lupker, M. et al. Predominant floodplain over mountain weathering of Himalayan sediments (Ganga basin). *Geochim. Cosmochim. Acta* **84**, 410–432 (2012).
18. Bouchez, J. et al. Floodplains of large rivers: weathering reactors or simple silos? *Chem. Geol.* **332-333**, 166–184 (2012).
19. Dong, H. et al. A critical review of mineral-microbe interaction and co-evolution: mechanisms and applications. *Natl. Sci. Rev.* **9**, nwac128 (2022).
20. Hoving, A. L. et al. What does mediated electrochemistry reveal about regional differences in the redox properties of Boom Clay? *Appl. Geochem.* **120**, 104681 (2020).
21. Zheng, Y. et al. Refractory humic-like substances: tracking environmental impacts of anthropogenic groundwater recharge. *Environ. Sci. Technol.* **54**, 15778–15788 (2020).
22. Dickens, A. F., Baldock, J., Kenna, T. C. & Eglinton, T. I. A depositional history of particulate organic carbon in a floodplain lake from the lower Ob' River, Siberia. *Geochim. Cosmochim. Acta* **75**, 4796–4815 (2011).
23. Feng, X. et al. Electrochemistry and molecular compositions reflect electron shuttling of dissolved organic matter in high arsenic groundwater. *Environ. Sci. Technol.* **59**, 8591–8601 (2025).
24. Zhao, L. D. et al. Biological redox cycling of iron in nontronite and its potential application in nitrate removal. *Environ. Sci. Technol.* **49**, 5493–5501 (2015).

25. Byrne, J. M. et al. Redox cycling of Fe(II) and Fe(III) in magnetite by Fe-metabolizing bacteria. *Science* **347**, 1473–1476 (2015).
26. Klupfel, L., Piepenbrock, A., Kappler, A. & Sander, M. Humic substances as fully regenerable electron acceptors in recurrently anoxic environments. *Nat. Geosci.* **7**, 195–200 (2014).
27. Zhang, N. et al. Water table fluctuations regulate hydrogen peroxide production and distribution in unconfined aquifers. *Environ. Sci. Technol.* **54**, 4942–4951 (2020).
28. Aeppli, M. et al. Export of organic carbon from reduced fine-grained zones governs biogeochemical reactivity in a simulated aquifer. *Environ. Sci. Technol.* **56**, 2738–2746 (2022).
29. Joshi, P., Schroth, M. H. & Sander, M. Redox properties of peat particulate organic matter: quantification of electron accepting capacities and assessment of electron transfer reversibility. *J. Geophys Res: Biogeosci.* **126**, e2021JG006329 (2021).
30. Huang, J. Z. et al. Fe(II) redox chemistry in the environment. *Chem. Rev.* **121**, 8161–8233 (2021).
31. Zhang, P. et al. Kinetic models for hydroxyl radical production and contaminant removal during soil/sediment oxygenation. *Water Res.* **240**, 120071 (2023).
32. Yu, C. et al. Mechanistic insight into humic acid-enhanced hydroxyl radical production from Fe(II)-bearing clay mineral oxygenation. *Environ. Sci. Technol.* **55**, 13366–13375 (2021).
33. Hoving, A. L., Sander, M., Bruggeman, C. & Behrends, T. Redox properties of clay-rich sediments as assessed by mediated electrochemical analysis: separating pyrite, siderite and structural Fe in clay minerals. *Chem. Geol.* **457**, 149–161 (2017).
34. Brookshaw, D. R., Coker, V. S., Lloyd, J. R., Vaughan, D. J. & Pattrick, R. A. D. Redox interactions between Cr(VI) and Fe(II) in bioreduced biotite and chlorite. *Environ. Sci. Technol.* **48**, 11337–11342 (2014).
35. Bishop, M. E., Dong, H. L., Kukkadapu, R. K., Liu, C. X. & Edelmann, R. E. Bioreduction of Fe-bearing clay minerals and their reactivity toward pertechnetate (Tc-99). *Geochim. Cosmochim. Acta* **75**, 5229–5246 (2011).
36. Xie, W. J. et al. Contaminant degradation by •OH during sediment oxygenation: dependence on Fe(II) species. *Environ. Sci. Technol.* **54**, 2975–2984 (2020).
37. Kurek, M. R. et al. High voltage: the molecular properties of redox-active dissolved organic matter in northern high-latitude lakes. *Environ. Sci. Technol.* **57**, 8617–8627 (2023).
38. Tan, W. et al. Increased electron-accepting and decreased electron-donating capacities of soil humic substances in response to increasing temperature. *Environ. Sci. Technol.* **51**, 3176–3186 (2017).
39. Yuan, X. et al. Production of hydrogen peroxide in groundwater at Rifle, Colorado. *Environ. Sci. Technol.* **51**, 7881–7891 (2017).
40. Li, Q., Zhang, C. & Shan, B. Stability of sedimentary organic matter: Insights from molecular and redox analyses. *Environ. Sci. Ecotechnol.* **22**, 100470 (2024).
41. Qiao, J. T. et al. Humic substances facilitate arsenic reduction and release in flooded paddy soil. *Environ. Sci. Technol.* **53**, 5034–5042 (2019).
42. Xiao, J. et al. The molecular weight-dependent redox capacity of soil dissolved organic matter: Roles of aromaticity and organic sulfur. *Geochim. Cosmochim. Acta* **401**, 174–189 (2025).
43. Walpen, N., Getzinger, G. J., Schroth, M. H. & Sander, M. Electron-donating phenolic and electron-accepting quinone moieties in peat dissolved organic matter: quantities and redox transformations in the context of peat biogeochemistry. *Environ. Sci. Technol.* **52**, 5236–5245 (2018).
44. Freeman, C., Ostle, N. & Kang, H. An enzymic 'latch' on a global carbon store. *Nature* **409**, 149–149 (2001).
45. LaRowe, D. E. & Van Cappellen, P. Degradation of natural organic matter: A thermodynamic analysis. *Geochim. Cosmochim. Acta* **75**, 2030–2042 (2011).
46. Zhou, C. X., Liu, Y. D., Liu, C. X., Liu, Y. Y. & Tfaily, M. M. Compositional changes of dissolved organic carbon during its dynamic desorption from hyporheic zone sediments. *Sci. Total Environ.* **658**, 16–23 (2019).
47. Wu, T. et al. Isolation and microbial reduction of Fe(III) phyllosilicates from subsurface sediments. *Environ. Sci. Technol.* **46**, 11618–11626 (2012).
48. Kukkadapu, R. K. et al. Reductive biotransformation of Fe in shale–limestone saprolite containing Fe(III) oxides and Fe(II)/Fe(III) phyllosilicates. *Geochim. Cosmochim. Acta* **70**, 3662–3676 (2006).
49. Shi, L. et al. Molecular underpinnings of Fe (III) oxide reduction by Shewanella oneidensis MR-1. *Front. Microbiol.* **3**, 50 (2012).
50. Qian, A. et al. Mechanistic insight into electron transfer from Fe(II)-bearing clay minerals to Fe (hydr)oxides. *Environ. Sci. Technol.* **57**, 8015–8025 (2023).
51. Zhang, X. et al. Biogeochemical coupling of C/Fe in oil-polluted wetlands associated with iron reduction. *Commun. Earth Environ.* **6**, 77 (2025).
52. Liu, D. et al. Reduction of structural Fe(III) in nontronite by methanogen Methanosarcina barkeri. *Geochim Cosmochim. Acta* **75**, 1057–1071 (2011).
53. Obradović, N. et al. Peat particulate organic matter accepts electrons during in situ incubation in the anoxic subsurface of ombrotrophic bogs. *J. Geophys Res.* **129**, e2024JG008223 (2024).
54. Zhang, Y. et al. Greenhouse gases concentrations and emissions in different inland water bodies in Chengdu Plain. *Desalin Water Treat.* **239**, 101–117 (2021).
55. Sun, Z. et al. Effects of straw returning and feeding on greenhouse gas emissions from integrated rice-crayfish farming in Jianghan Plain, China. *Environ. Sci. Pollut. Res.* **26**, 11710–11718 (2019).
56. Tian, H. et al. The terrestrial biosphere as a net source of greenhouse gases to the atmosphere. *Nature* **531**, 225–228 (2016).
57. Egger, M. et al. Iron-mediated anaerobic oxidation of methane in Brackish coastal sediments. *Environ. Sci. Technol.* **49**, 277–283 (2015).
58. Petri, B. G. et al. Fundamentals of ISCO using persulfate. In: *In situ chemical oxidation for groundwater remediation* (eds Siegrist R. L., Crimi M., Simpkin T. J.). (Springer, New York, 2011).
59. Mustapha, N. A., Liu, H., Ibrahim, A. O., Huang, Y. & Liu, S. Degradation of aniline in groundwater by persulfate with natural subsurface sediment as the activator. *Chem. Eng. J.* **417**, 128078 (2021).
60. Liu, H. Z., Bruton, T. A., Doyle, F. M. & Sedlak, D. L. In situ chemical oxidation of contaminated groundwater by persulfate: decomposition by Fe(III)- and Mn(IV)-containing oxides and aquifer materials. *Environ. Sci. Technol.* **48**, 10330–10336 (2014).
61. Amonette, J. E. & Templeton, J. C. Improvements to the quantitative assay of nonrefractory minerals for Fe(II) and total Fe using 1,10-phenanthroline. *Clays Clay Min.* **46**, 51–62 (1998).
62. He, C. et al. In-house standard method for molecular characterization of dissolved organic matter by FT-ICR mass spectrometry. *ACS Omega* **5**, 11730–11736 (2020).

Acknowledgements

This research was supported by the National Key R&D Program of China (2023YFC3706502, 2024YFC3712700) and the National Natural Science Foundation of China (U22A20591, 42577089). We would like to thank Prof. Dr. Chao Li from Chengdu University of Technology for his valuable discussions and insights on this paper.

Author contributions

C. Y., S. P., and F. W. designed the research. B. L. and L. F. performed most of the experiments. P. Z. supported the methodology for EEC analysis. C. Y., B. L., and L. F. performed data analysis. C. Y. and S. P. wrote and revised the paper. A. K., F. W., and P. Z. reviewed and edited the paper. S. P. and C. Y. funded the research.

Competing interests
The authors declare no competing interests.

Additional information
Supplementary information The online version contains supplementary material available at https://doi.org/10.1038/s43247-026-03307-3.

Correspondence and requests for materials should be addressed to Shengyan Pu or Fengchang Wu.

Peer review information *Communications Earth and Environment* thanks Peter Kraal and David J Burdige for their contribution to the peer review of this work. Primary Handling Editors: Mojtaba Fakhraee and Nandita Basu. [A peer review file is available].